Spatially resolved multiomics on the neuronal effects induced by spaceflight

Yuvarani Masarapu
Science for Life Laboratory, Department of Gene Technology, KTH Royal Institute of Technology
Egle Cekanaviciute
NASA
Zaneta Andrusivova
KTH Royal Institute of Technology
Jakub Orzechowski Westholm
Stockholm University https://orcid.org/0000-0002-6849-6220
Åsa Björklund
Uppsala University https://orcid.org/0000-0003-2224-7090
Robin Fallegger
Heidelberg University, Faculty of Medicine & Heidelberg University Hospital https://orcid.org/0000-0003-3264-6028
Pau Badia-i-Mompel
Heidelberg University https://orcid.org/0000-0002-1004-3923
Valery Boyko
NASA Ames Research Center
Shubha Vasisht
Department of Biomedical and Health Informatics, The Children's Hospital of Philadelphia Research Institute,
Amanda Saravia-Butler
NASA Ames Research Center
Samrawit Gebre
KBR/NASA Ames Research Center
Enikö Lázár
SciLifeLab, KTH Royal Institute of Technology https://orcid.org/0000-0001-8664-7531
Olaf Bergmann
Karolinska Institute https://orcid.org/0000-0003-1065-4107
Deanne Taylor
Children's Hospital of Philadelphia
Douglas Wallace
Children's Hospital of Philadelphia https://orcid.org/0000-0002-7480-8278
Christer Sylvén

Karolinska Institutet
Julio Saez Rodriguez
Heidelberg University https://orcid.org/0000-0002-8552-8976
Jonathan Galazka
NASA Ames Research Center https://orcid.org/0000-0002-4153-0249
Sylvain Costes
NASA Ames Research Center https://orcid.org/0000-0002-8542-2389
Stefania Giacomello (stefania.giacomello@scilifelab.se)
SciLifeLab, KTH Royal Institute of Technology https://orcid.org/0000-0003-0738-1574

Biological Sciences - Article

Keywords:

Posted Date: May 31st, 2023

DOI: https://doi.org/10.21203/rs.3.rs-2865086/v1

Additional Declarations: Yes there is potential Competing Interest. ZA and SG are scientific advisors to 10x Genomics Inc, which holds IP rights to the ST technology. S.G. holds 10X Genomics stock options. All other authors declare no competing interests.

Spatially resolved multiomics on the neuronal effects induced by spaceflight

Yuvarani Masarapu[1#], Egle Cekanaviciute[2#], Zaneta Andrusivova[1#], Jakub O. Westholm[3], Åsa Björklund[4], Robin Fallegger[5], Pau Badia-i-Mompel[5], Valery Boyko[2], Shubha Vasisht[6], Amanda Saravia-Butler[2], Samrawit Gebre[2], Enikö Lázár[7,8], Olaf Bergmann[7], Deanne M Taylor[6,9], Douglas C. Wallace[9], Christer Sylven[10], Julio Saez-Rodriguez[5], Jonathan M. Galazka[2*], Sylvain V. Costes[2*], Stefania Giacomello[1*]

[1]Science for Life Laboratory, Department of Gene Technology, KTH Royal Institute of Technology, Stockholm, Sweden

[2]NASA Ames Research Center, Moffett Field, CA 94035, USA

[3]National Bioinformatics Infrastructure Sweden, Department of Biochemistry and Biophysics, Stockholm University, Science for Life Laboratory, Stockholm, Sweden

[4]Department of Cell and Molecular Biology, National Bioinformatics Infrastructure Sweden, Science for Life Laboratory, Uppsala University, Uppsala, Sweden

[5]Heidelberg University, Faculty of Medicine, and Heidelberg University Hospital, Institute for Computational Biomedicine, Bioquant, Heidelberg, Germany

[6]Department of Biomedical and Health Informatics, The Children's Hospital of Philadelphia Research Institute, Philadelphia, PA, USA

[7]Department of Cell and Molecular Biology, Karolinska Institute, Stockholm, Sweden

[8]Department of Gene Technology, KTH Royal Institute of Technology, Science for Life Laboratory, Solna, Sweden

[9]Department of Pediatrics, The University of Pennsylvania Perelman School of Medicine, Philadelphia, PA, 19104, USA

[10]Department of Medicine, Karolinska Institute, Huddinge, Sweden

[#]first shared author

[*]corresponding authors: jonathan.m.galazka@nasa.gov, sylvain.v.costes@nasa.gov, stefania.giacomello@scilifelab.se

Abstract

Impairment of the central nervous system (CNS) functions in astronauts is a major health risk for long-duration space missions. Here, for the first time, we combine single-cell multiomics (transcriptomics and chromatin accessibility) and spatial transcriptomics analyses to discover spaceflight-mediated changes in the mouse brain. By comparing ground control and spaceflight animals, we found that the main processes affected by spaceflight include neurogenesis, synaptogenesis and synaptic transmission in cortex, hippocampus, striatum and neuroendocrine structures as well as astrocyte activation and immune dysfunction. At the pathway level, spaceflight resembles neurodegenerative diseases with oxidative stress and protein misfolding components, such as in Parkinson's disease. Our integrated spatial multiomics approach reveals both widespread and localized brain impairments and suggests key structures and mechanisms to be targeted for countermeasure development. All datasets can be mined through an interactive data portal as well as the National Aeronautics and Space Administration (NASA) GeneLab repositories.

Introduction

In preparation for the upcoming long-duration lunar and Mars missions, it is crucial to investigate the health risks to astronauts from exposure to spaceflight [1]. The key physiological impairments caused by the spaceflight environment include DNA damage and oxidative stress from galactic cosmic radiation [2], bone and muscle damage from gravitational changes [3,4], circadian and sleep dysregulation [5], microbial dysbiosis [6] and tissue and organ degeneration, including cardiovascular and CNS damage [7]. Studies on animal models have shown several spaceflight stressors directly impacting brain molecular mechanisms causing neuroinflammation, neurodegeneration and neurovascular damage [8–11]. Specifically, exposure to simulated space radiation levels, comparable to the ones expected during the planned Mars mission, leads to neurodegeneration and neuroinflammation *in vivo* and in tissue and cell models [12], as well as cognitive and behavioral deficits in rodent models.

Major physiological effects of microgravity in low-Earth orbit, such as at the International Space Station (ISS), include a shift of body fluids from lower towards upper parts of the body, which leads to cardiovascular [13] and CNS changes [14]. Other environmental changes, including circadian and sleep dysregulation and microbial dysbiosis, have also been reported both in astronauts and in model organisms [5,15], though the extent of their contribution to degenerative CNS impairments remains to be investigated at greater depth.

Although studies performed directly on astronauts are the most relevant, they have to be minimally invasive, resulting in limited information on molecular and cellular level outcomes, while rodent models allow for the investigation of spaceflight effects using entire organs.

In this study, we explored spaceflight-induced molecular changes in brain tissue using spatial and multiomics approaches on young adult female BALB/c mice samples obtained during

the Rodent Research-3 (RR-3) mission and requested from the NASA Biological Institutional Scientific Collection (NBISC). We combined single-nucleus multiomics (i.e., snMultiomics, RNA and ATAC sequencing) with Spatial Transcriptomics (ST) data to study changes at DNA and RNA level in the context of different brain regions. We discovered many brain regions that could be spatially mapped with the identified clusters from both the ST and the combined single-nucleus multiomics datasets (detailed description in **Results** section). We also found, at the clusters and pathway level, many differences induced by spaceflight (see **Results**).

Single cell sequencing technologies are powerful methods to discover novel cell types and/or to obtain information about cell type composition of a tissue type based on gene expression of each cell. However, the applicability of single cell transcriptomics relies on the accessibility of fresh specimens and the possibility to successfully dissociate the tissue of interest [16]. Since sample preparation in spaceflight studies typically uses in-orbit freezing of the whole carcass in order to simplify the experiment and minimize crew time, studying single nuclei transcriptomics becomes the method of choice instead. By isolating nuclei from tissue block we are able to measure transcriptomics profiles of each nucleus which we can further use to study differences between flight and ground control. Furthermore, we were able to evaluate both transcriptional profiles and chromatin changes in the same nuclei, providing paired data on both RNA and DNA level. On the other hand, while single nuclei sequencing methods give us the possibility to study transcriptomes of individual nuclei, the spatial context is lost. Therefore, applying spatial transcriptomics can be a powerful add-on to study changes in their spatial location in order to obtain transcriptomics information coupled with its original location within tissue section [17].

To our knowledge, this is the first study combining spatial and single nuclear omics techniques to understand molecular changes induced by the space environment at the resolution of

individual cell type and brain region. Thus, in addition to biological findings, our work might also be used as a stepping stone for experimental design of follow up spaceflight mission studies.

Results

To identify specific cellular microenvironments affected by spaceflight, we apply Spatial Transcriptomics (ST; 10X Genomics Visium) and single-nucleus multiomics (snMultiomics; gene expression and chromatin accessibility; 10x Genomics Single Cell Multiome ATAC + Gene Expression) on mouse brain. In total, we analyzed three brains from mice euthanized on-board the International Space Station (ISS; F1, F2, F3) and three brains from ground control mice (G1, G2, G3) that were kept under matched conditions. For each sample, we isolated nuclei from one hemisphere for snMultiomics analysis and cryo-sectioned the other hemisphere in the hippocampal region for ST analysis (**Fig. 1**).

Spaceflight sample quality is suitable for ST and snMultiomics analysis

As a first step, we ensured that the morphological and RNA quality of the samples was preserved well enough for our experimental workflow given that our spaceflown samples had to undergo a specific preservation approach[18], which was also adopted for the corresponding ground control animals. In brief, to preserve changes induced by the space environment, spaceflown mice were euthanized on-board the ISS and underwent freezing as a whole carcass in a -80°C freezer. Upon return to Earth, the carcasses were partially thawed to enable organ dissection followed by a second round of snap freezing of individual organs. We measured the RNA integrity number (RIN) for each sample (**Supplementary Fig. 1A**) and found that it was 9.15 on average.

Furthermore, we performed a tissue optimization experiment (see **Methods**, **Supplementary Fig. 1B**) confirming that both morphology and RNA was of sufficient quality for ST analysis.

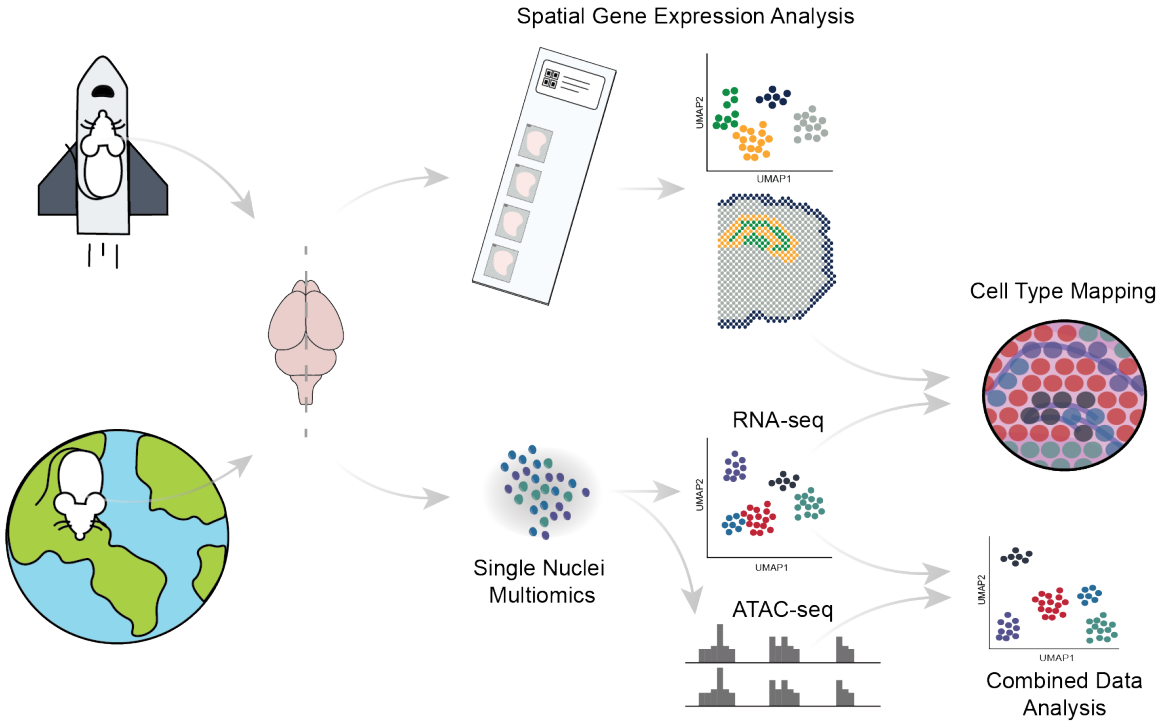

Fig. 1: Summary of the project workflow.

snMultiomics identifies distinct cell types in spaceflown mouse brains

To dissect the neuronal alterations induced by spaceflight at the single-cell level, we performed a snMultiomics analysis on hemispheres of three spaceflown (F1, F2, F3) mice and two ground controls (G2, G3), thus obtaining RNA expression profiles and chromatin accessibility (ATAC) information from the same nucleus.

In total, we isolated 21,178 nuclei across the spaceflight and control samples with an average of 3,140 UMIs/nucleus (snRNA-seq) and 9,217 peaks/nucleus (snATAC-seq) (**Fig. 2A, B, Supplementary Fig. 1C**) and a high gene expression correlation between the spaceflight and

ground control samples ($r=0.95$, $p<0.05$; **Fig. 2C**). By integrating and performing a joint clustering analysis of the snRNA-seq and snATAC-seq datasets (further referred to as "multiomics"), we identified 18 clusters (**Fig. 2D, Supplementary Fig. 2**). By leveraging previously reported marker genes in the literature (See 'Gene Annotation' under **Methods** section for details), we identified 11 macro categories for the 18 multiomics clusters (interchangeably referred to as 'sn clusters' in the next sections) according to their functions (**Fig. 2E, Supplementary Table 1, 2**). The majority of clusters were related to neurogenesis, neuronal activity and synaptic transmission, distinguished by functional differences in synaptic connections (GABAergic, glutamatergic, dopaminergic) and neuronal locations (neuroendocrine, striatal, cortical, hippocampal).

We identified a total of 825 differentially expressed genes (DEGs) induced by spaceflight across the sn clusters (**Supplementary Table 3**), with the highest number of DEGs (381 in total) found in sn cluster 5 (Glutamatergic Synaptic Transmission I) and lowest number of DEGs (1 gene) in sn cluster 2 (Neuronal activity, Synaptic Transmission I) and sn cluster 7 (Glial Development). The majority of these 825 DEGs were involved in neuronal development (sn clusters 9, 11), axonal dendritic development (sn clusters 9, 14), synaptic transmission (sn clusters 4, 5, 14) and GABAergic synaptic transmission (sn cluster 11). Notably, 28 DEGs were shared between sn clusters 5, 11, and 14. Consensus pathway analysis [19] showed a significant change in pathways encoding synaptic plasticity and synaptic transmission as well as the circadian entrainment of synaptic functions, suggesting a disruption of circadian rhythm in spaceflight, a known stressor in spacecraft due to the lack of natural light.

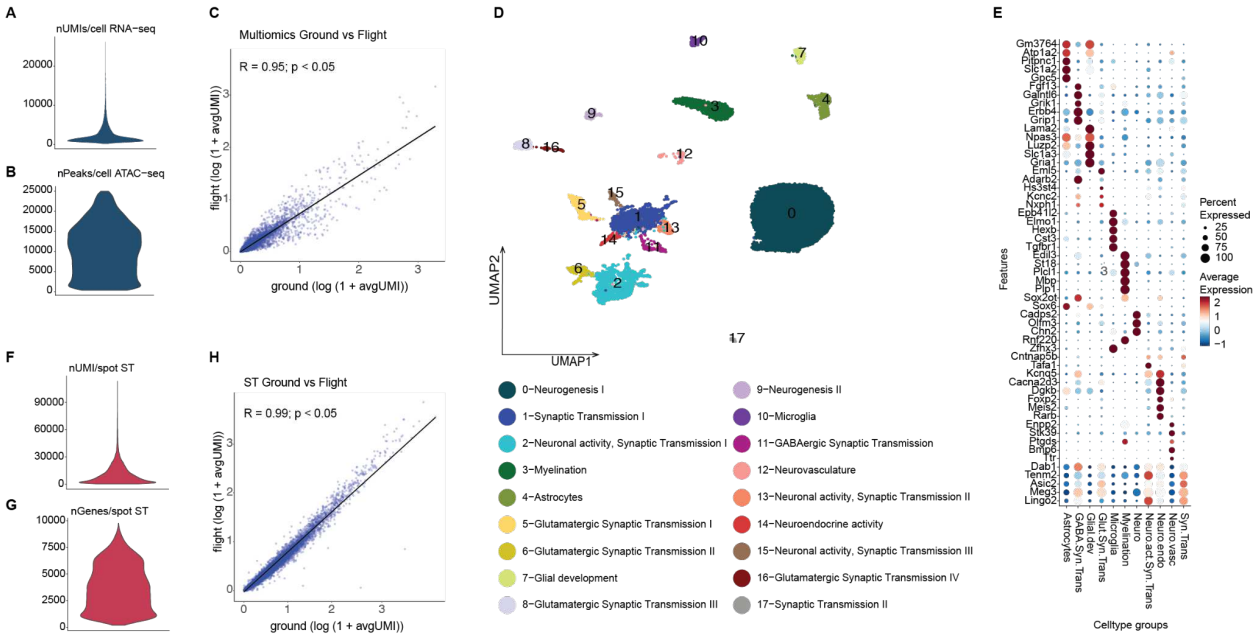

151

152 **Fig. 2: Single-nucleus multiomics analysis of spaceflown mouse brains. A,** Distributions of
153 UMIs per nucleus in snRNA-seq dataset. **B**, Distribution of peaks per nucleus in snATAC-seq
154 dataset. **C**, Correlation plot between flight (y-axis) and ground control (x-axis) single nuclei
155 multiomics samples. **D,** UMAP of single nuclei multiomics data and cluster annotations. **E,** 11
156 functional multiomics clusters represented by their marker genes. **F,** Distributions of UMIs per
157 spot for the whole spatial transcriptomics dataset. **G**, Distribution of unique genes per spot for
158 the whole spatial transcriptomics dataset. **H,** Correlation between flight (y-axis) and ground
159 control (x-axis) ST samples.

160

161 ***ST provides a high-resolution mapping of mouse brain regions***

162 To investigate spaceflight-induced neuronal alterations at a spatial level, we performed ST
163 analysis on the other brain hemispheres. To increase statistical robustness, we added an additional

ground control sample (G1). We collected two coronal sections from each brain hemisphere containing hippocampus, somatosensory cortex, striatum, amygdala and corpus callosum.

In total, we captured 14,630 genes across 29,770 spots after filtering and detected 10,884 UMIs/spot and 3,755 genes/spot on average (**Fig. 2F,G, Supplementary Fig. 3A,B**) and found a high gene expression correlation between the spaceflight and ground control tissue sections ($r=0.99$, $p<0.05$; **Fig. 2H**). Our unsupervised clustering analysis of the spot information identified 18 distinct spatial clusters (further referred as 'ST clusters') (**Fig. 3A,B and Supplementary Table 4**), which presented a clear separation between the cortical top (ST cluster 1) and bottom layers (ST cluster 9), as well as other major structures, including hippocampus (with separation of CA1, CA3, dentate gyrus in ST clusters 10, 8 and 11 respectively), thalamus (ST cluster 5), striatum (ST clusters 0, 14), hypothalamus (ST cluster 2), pituitary (anterior and posterior; ST cluster 2), corpus callosum (ST cluster 12) and cerebral peduncles (ST cluster 4) (**Fig. 3C**). The key functions of the markers (**Supplementary Table 5**) that were repeated among numerous ST clusters include neurogenesis, neuronal development, axonal growth and synaptogenesis.

Next, we investigated how spaceflight influences gene expression at the spatial level and identified a total of 4057 DEGs for spaceflight in 7 ST clusters (**Supplementary Table 6**). Specifically, 18 DEGs in Caudate/putamen neurons (ST cluster 14) are related to neuronal development, synaptogenesis, synaptic plasticity and to a lesser extent, neurodegeneration. Similarly, Hippocampal CA3 neurons (ST cluster) showed a total of 21 DEGs known to be involved in neurogenesis, synaptogenesis and neurodegeneration. Cortical neurons (bottom layers; ST cluster 9) showed an abundance of DEGs (3208 in total; 1808 upregulated and 1400 downregulated) with functions related to neuronal development, and synaptic transmission in the bottom layers of cortex (somatosensory, motor, visual). Consensus pathway analysis[19] highlighted

multiple neurodegeneration-associated pathways in Cortical neurons (bottom layers; ST cluster 9) and Choroid plexus and subventricular structures (ST cluster 16), including protein misfolding and abnormal protein clearance, mapping to neurodegenerative diseases characterized by protein misfolding and accumulation, such as Parkinson's disease, Alzheimer's disease and Huntington's disease [20,21] (**Fig. 3D,E**).

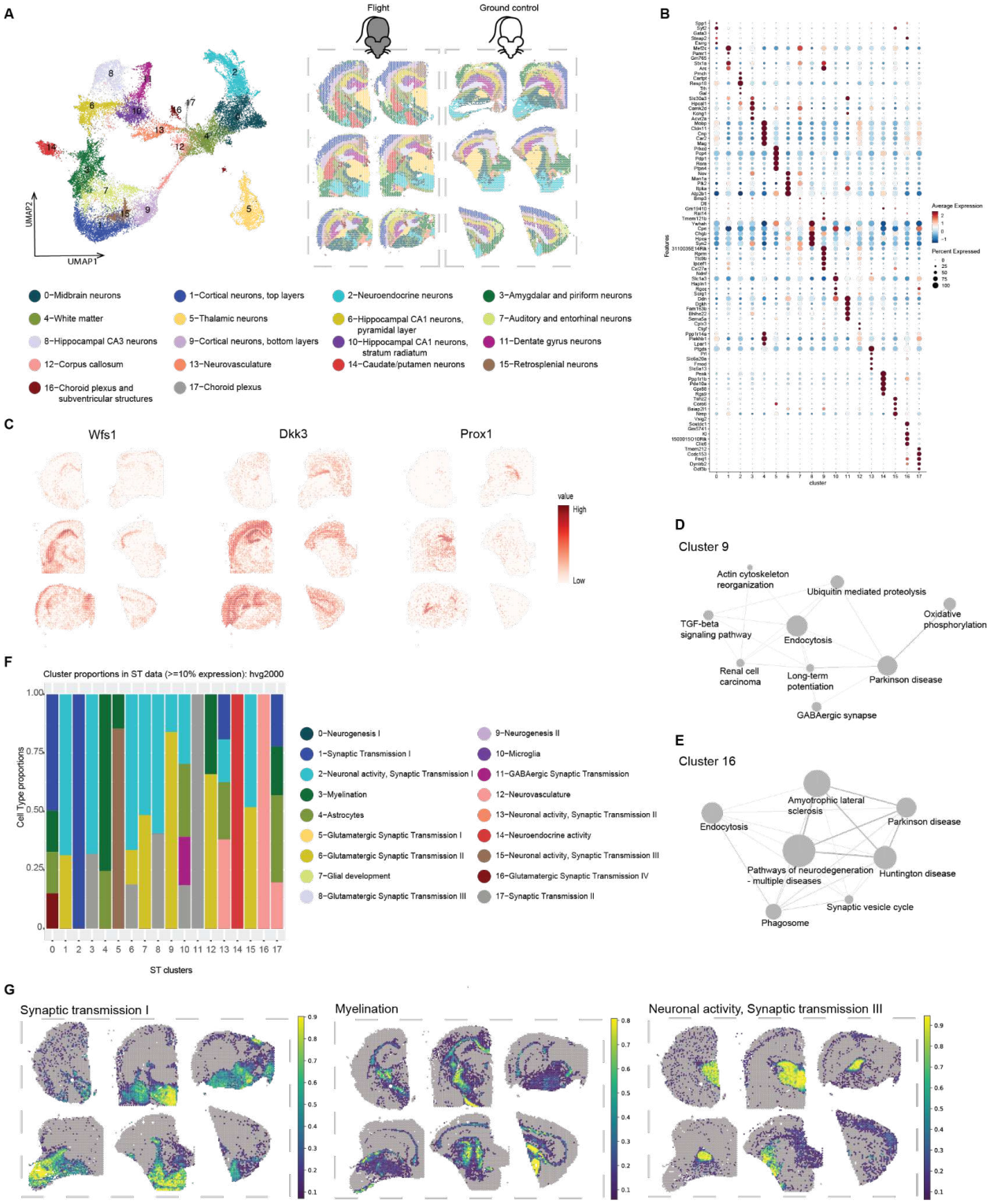

Figure 3: Spatial Transcriptomics datasets, cell type deconvolution and pathway analysis of ST data. A, Clustering of spatial transcriptomics data, cluster annotations and spatial location of

clusters visualized on flight and ground control mouse brain sections. **B,** Marker genes for each ST cluster visualized as dotpot. **C,** Spatial distribution of 3 genes (Wfs1 for CA1 region of hippocampus, Dkk3 for CA1 and CA3 hippocampal region and Prox1 for Dentate gyrus). **D,** Significantly different pathways between flight and ground control in ST cluster 9 (Cortical neurons, bottom layers). **E,** Significantly different pathways between flight and ground control in ST cluster 16 (Choroid plexus and subventricular structures). **F,** Visualization of number of clusters identified by multiomics and their proportions in each ST cluster. **G**, Cell type proportion mapped to spatial coordinates on ground and flight mouse brain sections (Synaptic transmission I or sn cluster 1, Myelination or sn cluster 3 and Neuronal activity, Synaptic transmission III or sn cluster 15).

Integration of multiomics and ST datasets indicates spaceflight effects on synaptic transmission

To infer the spatial distribution of the clusters identified in the multiomics dataset, we performed a spot deconvolution analysis on the matching ST dataset using software called Stereoscope[22] (**Fig. 3F**). The deconvolution analysis revealed functional similarities between several multiomics and spatial data clusters, for instance, clusters encoding synaptic transmission (sn cluster 1 and ST clusters 0, 2), myelination in white matter (sn cluster 3 and ST cluster 4, 12), and neuronal development (sn cluster 15 and ST cluster 5) (**Fig. 3G; Supplementary Fig. 5, 6; Supplementary Table 7**). The similarities identified from the deconvolution highlighted similar outcomes of spaceflight in the multiomics and spatial clusters: disrupted synaptic transmission in cortex (including both neurons and astrocytes, as revealed by snRNA-seq data that allowed cell type separation) and neurodevelopment, especially of dopaminergic neurons in striatum.

Ligand-receptor interaction analysis suggests spaceflight-mediated effects on astrocyte functions

To assess the effects of spaceflight on the cell-cell interaction level, we performed a ligand-receptor analysis on the multiomics clusters that showed the most differentially expressed genes in response to spaceflight, i.e., sn clusters 4 (Astrocytes), 5 (Glutamatergic Synaptic Transmission I), 11 (GABAergic Synaptic Transmission), and 14 (Neuroendocrine activity). We found 9 interactions significantly upregulated (**Fig. 4A**). These included adhesion molecule pairs, EGFR (epidermal growth factor receptor) pairs, PTN (pleiotrophin, a heparin-binding brain mitogen), EFNA5 (ephrin A5, ligand for tyrosine kinase Eph receptors), and VEGFA (vascular endothelial growth factor). All molecules have previously been shown to be involved in cellular development in the CNS. PTN[23] is a general developmental regulator, while adhesion molecule, EGFR[24], is involved in neuronal development, including axonal outgrowth. Instead, VEGFA[25,26] primarily regulates angiogenesis and endothelial cell functions, though is also involved in synapse formation and functions. No ligand-receptor interactions in these clusters were significantly downregulated.

Interestingly, we found that spaceflight increased VEGFA_GRN28 interactions between sn cluster pairs 4-14 (Astrocytes-Neuroendocrine activity), 4-11 (Astrocytes-GABAergic Synaptic Transmission), 4-5 (Astrocytes-Glutamatergic Synaptic Transmission I), 5-11 (Glutamatergic Synaptic Transmission I-GABAergic Synaptic Transmission) and 5-14 (Glutamatergic Synaptic Transmission I-Neuroendocrine activity). Primarily astrocyte-produced VEGFA has previously been demonstrated to regulate the NMDA receptor activity [26,27]. In the adult brain, VEGFA acts as a neurogenic factor augmenting cell proliferation, neuroblast production and neuronal differentiation in the hippocampus [25].

In addition, we found sn cluster 4 (Astrocytes) and sn cluster 11 (Glutamatergic Synaptic Transmission I) interacting with sn cluster 14 (Neuroendocrine activity) via the EGFR_NRG1 pair. EGFR is a member of the tyrosine kinase superfamily and is known to be involved in maintenance and regeneration after injury. It is also known to be associated with neurodegenerative diseases such as Parkinson's disease, Alzheimer's disease and amyotrophic lateral sclerosis [24].

Motif analysis unravels spaceflight effects on Transcription Factor (TF) activity

To investigate the effects of spaceflight on Transcription Factors (TFs), we performed motif analysis on snATAC-seq peaks from the multiomics data. The motif analysis revealed differences in activity of TFs between the flight and ground control brain samples in several sn clusters (**Supplementary Table 8**). Many motifs were repeated notably across sn clusters 4 (Astrocytes), 11 (Glutamatergic Synaptic Transmission I) and 14 (Neuroendocrine activity). Specifically, spaceflight samples showed a reduced accessibility of motifs Zic1, Zic2 and Atoh1 in sn clusters 4 (Astrocytes) and 14 (Neuroendocrine activity), suggesting a decrease in astrocytic functions and neuronal activity in the telencephalon interneurons, respectively [28,29]. Meanwhile, increased accessibility of motifs Pou5f1 and Sox2 in sn cluster 11 (Glutamatergic Synaptic Transmission I) might indicate a potential increase in the pluripotency of neuronal progenitor cells and reduced neuronal differentiation in telencephalon interneurons in spaceflight [30–32]. Similar outcomes were suggested by spaceflight-mediated reduction in accessibility for NR4A2 motif in sn cluster 14 (Neuroendocrine activity), an important motif for differentiation and maintenance of dopaminergic neurons [33] (**Fig. 4B**).

In addition to neuronal effects, motifs Pparg, Rxra and Nr2f6, known to repress NFkB, innate immune responses to viruses and hormone and immune responses, respectively, showed

decreased accessibility in telencephalon interneurons (sn cluster 11), suggesting increased inflammatory responses [34–36]. Finally, we detected a decreased accessibility for Hic1, a p53 DNA damage response regulator motif that downregulates SIRT1, in sn cluster 14 (Neuroendocrine activity), which might be associated with increased DNA damage in spaceflight [37]. This motif, along with Pparg, Rxra and Nr2f6 is also known to be associated with both systemic and CNS-specific circadian rhythms, suggesting a possible circadian dysregulation induced by spaceflight [38–42].

Differential spatial patterns show several changes in signaling pathways occurring in spaceflight brain samples

Local environments of specific celltypes or groups of spots may have changes in pathway signaling, and in order to investigate this, we leveraged the spatially-resolved cell type deconvolution results from Stereoscope. We analyzed the ST dataset for tissue remodeling as well as changes in pathway signaling upon spaceflight using the Multiview intercellular SpaTial modeling framework (MISTy)[43]. This tool allowed us to investigate the relationships between cell type proportions in each ST spot and activities of 14 pathways inferred by decoupler-py and PROGENy [44,45]. Specifically, the MISTy models predict the cell type abundance in a spot (inferred with Stereoscope from the multiomics clusters) from a so-called intraview (features in the same spot) and from a paraview (weighted sum of the features in the neighboring spots; weights decreasing with distance). The features were either the cell type abundances of the other cell types to investigate changes in tissue structure or pathway activities to study changes in signaling. A separate model was built for each cell type and for each sample. In order to identify changes

induced by spaceflight, we aggregated the models and looked for predictors important in flight samples, but not in ground controls, and vice-versa.

Based on the models using cell type abundances as predictors, we were unable to find any evidence of changes in cell type colocalization events between flight and ground controls. This is also supported by the fact that there are no overall changes in cell type abundance from the deconvolution results (**Supplementary Fig. 5 and 6**), which is expected for tissue restructuring or lesion formation.

In contrast, we were able to identify changes in signaling pathway activities associated with individual cell types. We found that cell abundance of the neurovasculature (sn cluster 12) colocalizes with decreased MAPK signaling in flight but not in ground controls (**Fig. 4C**). Similarly, we found signaling changes in the local neighborhood (MISTy paraview) of several other cell types in flight (**Fig. 4D**): (1) EGFR signaling is less negatively correlated with abundances of class IV glutamatergic neuronal cells in the di- and mesencephalon (sn cluster 16: Glutamatergic synaptic transmission IV); (2) MAPK is more negatively correlated with cholinergic, monoaminergic and peptidergic neurons (sn cluster 17: Synaptic transmission II); (3) higher TGFb signaling in the vicinity of GABAergic interneurons in the telencephalon (sn cluster 11: GABAergic synaptic transmission); (4) lower WNT activities around neurons of class II glutamatergic neurons (sn cluster 6: Glutamatergic synaptic transmission II).

In order to assess the downstream changes these signaling activities might have, we built a tissue-specific gene regulatory network (GRN) from the multiomics data using CellOracle[46]. From this network, we predicted TF activities in the spatial data and computed the Pearson correlation between TF and signaling activities for the dysregulated pathways in spots containing the cell types identified above. We found that the increased TGFb signaling around GABAergic interneurons

(sn cluster 11: GABAergic synaptic transmission) in the flight samples is associated with an increase and decrease in activity of Sox6 and Lmx1a, respectively (**Fig. 4E, F**).

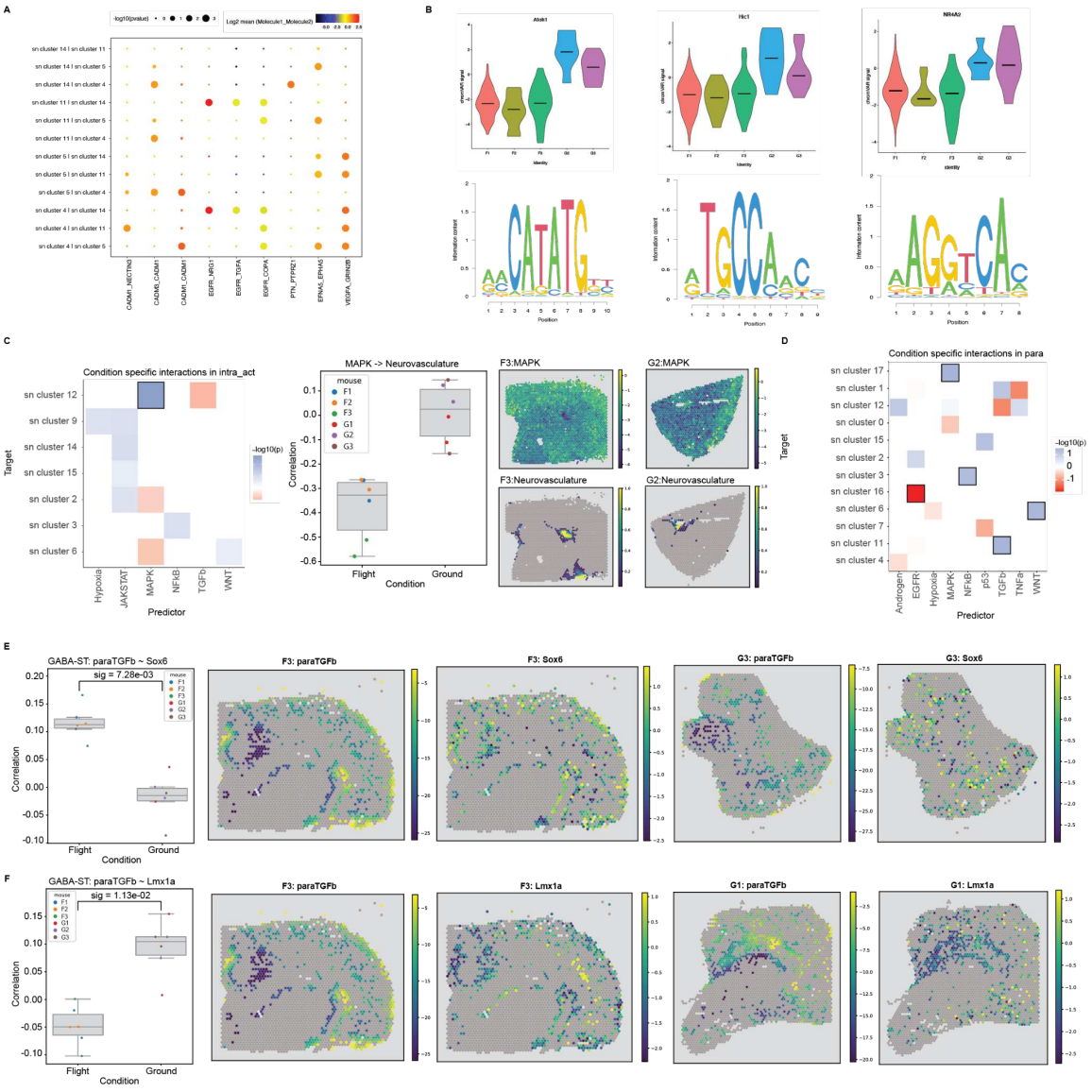

Figure 4: Ligand-receptor interactions, motif accessibility, and signaling pathways affected by spaceflight. A, Ligand receptor interactions for the spaceflight-affected multiomics clusters. **B,** Effects of spaceflight on motif accessibility (Atoh1, Hic1 and NR4A2 in cluster 14). **C,** (left) adjusted p-value of differential interactions found by MISTy in the intraview (cell type and

pathway activity colocalization) occuring only in flight (blue) or in controls (red), (middle) correlation of MAPK pathway activity and Neurovasculature abundance, and mapped on Visium slide for two samples (right). **D,** adjusted p-value of differential interactions found by MISTy in the paraview (cell type and pathway activity in local neighborhood) occuring only in flight (blue) or in controls (red), tiles with black border identify statistically significant changes**. E,** Correlation of Sox6 activity (left) within spots containing GABA-ST cells and TGFb activity in their local neighborhood (paraTGFb), respectively, and their respective activities in Visum slides (4 righternmost plots)**. F,** Correlation of Lmx1a activity (left) within spots containing GABA-ST cells and TGFb activity in their local neighborhood (paraTGFb), respectively, and their respective activities in Visum slides (4 righternmost plots).

Metabolic gene enrichment analysis shows decreased metabolic-related gene expression in spaceflight mice

Gene Set Enrichment Analysis (GSEA) on the ST data using metabolic pathways indicate an enrichment in genes with negative fold change (flight-vs-ground) yielding negative GSEA[47,48] normalized enrichment scores (NES) within the Oxidative Phosphorylation pathway, especially for genes related to Complex I (**Fig. 5A, Supplementary Table 9**). Other significantly affected pathways showing an FGSEA enrichment for genes with negative log2fold-change (i.e. reduced in spaceflight) in the spatial data (adjusted p-value <= 0.05) included Glycolysis/gluconeogenesis (**Supplementary Fig. 7**), Fructose and Mannose Metabolism (**Supplementary Fig. 8**) and Arachidonic acid Metabolism (**Fig. 5B**). In the multiomics data, those same pathways, in addition to Fatty Acid Synthesis (**Fig. 5C**) were also found to be reduced by spaceflight (**Supplementary Table 10**). The deficits in oxidative phosphorylation are consistent with previously reported

mitochondrial impairments caused by spaceflight [49], as well as the associations with neurodegenerative disease with a major oxidative stress component, such as Parkinson's Disease. Meanwhile, arachidonic acid is primarily produced by astrocytes as part of regulating blood flow in the brain based on physiological and metabolic state. Defects in astrocyte regulation of blood flow to the brain are also associated with neurodegeneration, including Alzheimer's Disease and Amyotrophic Lateral Sclerosis [50–53].

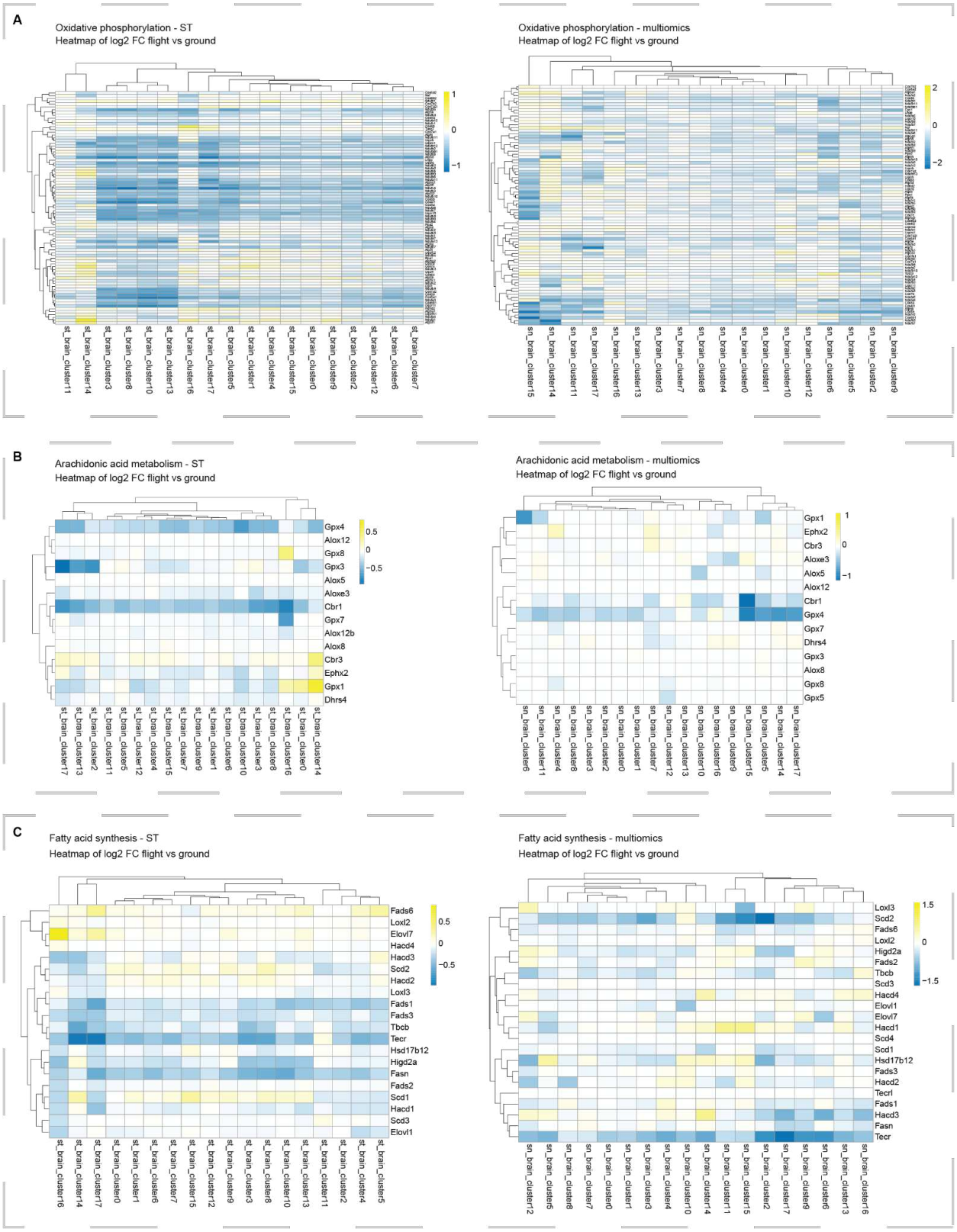
A
Oxidative phosphorylation - ST
Heatmap of log2 FC flight vs ground
Oxidative phosphorylation - multiomics
Heatmap of log2 FC flight vs ground
B
Arachidonic acid metabolism - ST
Heatmap of log2 FC flight vs ground
Arachidonic acid metabolism - multiomics
Heatmap of log2 FC flight vs ground
C
Fatty acid synthesis - ST
Heatmap of log2 FC flight vs ground
Fatty acid synthesis - multiomics
Heatmap of log2 FC flight vs ground

Figure 5: Metabolic gene set enrichment analysis A, Heatmap showing log2FC between flight and ground control samples in oxidative phosphorylation pathway in both ST and multiomics datasets. **B,** Heatmap showing log2FC between flight and ground control samples in Arachidonic acid metabolism pathway in both ST and multiomics datasets. **C,** Heatmap showing log2FC between flight and ground control samples in Fatty acid synthesis pathway in both ST and multiomics datasets.

Discussion

In this study, we used brain samples from ground control and spaceflown mice from the RR-3 mission to understand the consequences of the space environment on individual brain cells and brain regions. The main alterations induced by spaceflight included changes in synaptogenesis, neuronal development as well as neurodegeneration associated with impaired protein folding and clearance, which overlapped with some of the effects of aging and neurodegenerative diseases. In addition, we observed spaceflight-mediated circadian disruption and mitochondrial damage coupled with oxidative stress. To our knowledge, this is the first study applying these high resolution analysis techniques to study the effects of spaceflight on the CNS, and it might serve as a stepping stone towards comparative analysis of samples from other space missions, as well as for live animal return and reacclimation to Earth conditions. We demonstrate spatial transcriptomics and single nuclei multiomics datasets to be highly complementary. For example, the single-nucleus resolution permitted a better separation of glial cells into astrocytes and microglia, which were not distinguishable in ST dataset, due to the lower resolution of the method. On the other hand, using the spatial information coupled with gene expression data allowed us to

observe region-specific effects of spaceflight. Furthermore, our snATAC-seq analysis in transcription factor binding sites indicated immune dysfunction in addition to spaceflight-mediated impairments of neurogenesis and synaptogenesis. Finally, analysis of ligand-receptor interactions revealed interactions between different cell clusters that were putatively important for adaptations during spaceflight, with the focus on neurodevelopment and astrocyte functions.

In our study, multiple lines of evidence converged on spaceflight-mediated disruption of neurogenesis, neuronal development and synaptogenesis, especially dopaminergic synapse formation in the striatum. Similar spaceflight outcomes of increased pluripotency and reduced cell differentiation have previously been reported in spaceflown mouse bone samples [54] and in human stem cell models [55], indicating that it might be a systemic impairment that includes the CNS. In addition, neurogenesis has been shown to be affected in a spaceflight analog study that combined simulated microgravity and low dose rate photon irradiation in mice [10], while synaptogenesis is particularly sensitive to simulated galactic cosmic radiation components [56], which might thus exacerbate CNS damage in deep space missions. Our observations in the striatal gene expression changes and transcription factor accessibility are novel and worth validating in future spaceflight experiments, since they might result in significant behavioral alterations due to disrupted dopaminergic signaling.

Spaceflight-associated changes in circadian gene expression are highly relevant considering that circadian disruption is defined as one of the major spaceflight stressors [57], though it has been comparatively little studied in spaceflight, especially in animal models [58]. Impairment of circadian rhythms has been shown to lead to immune dysfunction that resembles senescence in terrestrial models [59], and similar immune dysfunction has indeed been observed in spaceflight [60].

However, the molecular and cellular CNS correlation of circadian gene expression dysregulation in spaceflight remains to be investigated in greater detail.

Our results indicate multiple similarities between spaceflight and terrestrial CNS conditions. Synapse loss, oxidative stress, inflammation and protein misfolding observed in the striatum collectively resemble aging-associated neurodegeneration and Alzheimer's, Huntington's and Parkinson's diseases. Based on pathway analysis, the flight samples might particularly resemble Parkinson's Disease, indicating that anti-Parkinson's therapeutics might be repurposed as spaceflight countermeasures, or vice versa, that spaceflight could serve as an analog of accelerated aging-associated neurodegeneration [61]. Computational studies on identifying disorder analogs to alterations induced by spaceflight are ongoing, but have not yet included the CNS effects, which will require comparing the data from multiple spaceflight experiments [62].

In addition to validating the results of RR-3 mission by comparing them to the neuronal effects of spaceflight in other mouse studies at similarly high resolution, it will be important to expand the experimental profile to be able to address key aspects of astronaut health risks that have not been included yet. Among them, including a period of reacclimation to ground conditions will be crucial to quantify the extent to which spaceflight-mediated impairments persist after landing, especially as they are combined with the process of aging. In addition, the majority of mouse studies in spaceflight have been performed on females to facilitate group housing, while the astronaut cohort includes both male and female astronauts. Thus, it will be necessary to compare male and female outcomes to address the sexual dimorphism of CNS health risks. Finally, in order to extrapolate animal models to human outcomes, human and mouse CNS organ model systems will have to be flown as payloads. The first human neurovascular models have already been investigated on the ISS [63,64], though their results have not yet been published, while here, we

analyzed the effects of spaceflight on murine neurovasculature [65], highlighting the importance of astrocyte functions in missions beyond low-Earth orbit. In preparation for these missions, in which crew time will be severely limited, it will be essential to develop automated, long-lasting CNS models and compare their responses to model organisms. To facilitate the scientific community to use our datasets, all our data is openly available through NASA GeneLab and can be explored by a Shiny app (https://giacomellolabst.shinyapps.io/rr3-brain-shiny/).

Conclusion

In this study, we have combined spatial transcriptomics and single nuclei multiomics to analyze the neuronal effects of spaceflight on gene transcription in young female mice at the resolution of individual nuclei and distinct brain regions. We observed that spaceflight altered the expression of genes associated with neurogenesis, synaptogenesis and neuronal development in multiple regions of the brain, especially striatum, in addition to oxidative stress and neuroinflammation, as well as the barrier function of the choroid plexus. These effects resembled aging and neurodegenerative diseases at the pathway level, with particular similarity to Parkinson's Disease. Further studies using larger sample cohorts will be needed to validate these effects associated with the space environment and their persistence after landing.

Materials and Methods

Animals

A cohort of 12-week-old female BALB/c mice were flown to the ISS and housed in the Rodent Habitat for 39-42 days. Mice of similar age, sex and strain were used as ground controls housed in identical hardware and matching ISS environmental conditions, including but not limited to cage type, light cycle, food, temperature, humidity and CO_2 concentration. At the end of the mission, spaceflight and ground controls were euthanized and whole carcasses were stored at -80°C until the dissection on earth. Mouse carcasses were removed from -80°C storage and thawed at room temperature for 15-20 minutes for dissection. Each carcass dissection time was no longer than 1 hour from collection of the first tissue. Brain tissues were harvested and placed into 2 ml Eppendorf tubes for snap freezing in liquid nitrogen, then stored in -80°C freezer for sample processing.

RNA extraction

RNA was extracted from tissue sections using the RNeasy Mini kit (Qiagen). RNA integrity was measured by using the Agilent Bioanalyzer. All samples had RIN values above 8.

Sample preparation

Six brains in total, three from each group, were used in this study. Hemispheres of each of the brain samples were split. One hemisphere from each sample was embedded in Tissue-Tek O.C.T. and cryo-sectioned in the hippocampus area at 10 μm thickness. Sections were placed on Visium Gene Expression arrays, Superfrost glass slides or into Eppendorf tubes. Second hemisphere of each brain was used for nuclei isolation. Samples were stored in -80°C before processing.

Visium Spatial Gene Expression technology and sequencing

Spatial gene expression libraries were generated using the Visium Gene Expression kit (10x Genomics). Brain hemispheres were cryo-sectioned to reach the hippocampus area. Two consecutive sections of hippocampus from the ground control cohort and two consecutive sections of hippocampus from the flight cohort were placed on Visium glass slides. Consecutive sections were considered technical replicates. In total, 12 Visium libraries were prepared following the manufacturer's protocol (User Guide, CG000239 Rev F). Twelve libraries were sequenced by using an Illumina Novaseq platform, while four were sequenced on an Illumina NextSeq500 platform. and sequenced by using a Illumina Novaseq platform. Length of read 1 was 28 bp and read 2 was 120 bp long.

Chromium single-cell Multiome ATAC + Gene Expression technology and sequencing

Nuclei isolation

One hemisphere of 4 brains used for Spatial Transcriptomics was utilized for nuclei isolation. Brain tissue was placed into a tube together with lysis buffer (10mM Tris-HCl, 10nM NaCl, 3nM $MgCl_2$, 0.1% Igepal CA-630, 1mM DTT, 1U/µl RNAseOUT), homogenized by pestle homogenization in eppendorf tube and incubated on ice for 5 min. The nuclei were extracted by following 10XGenomic protocol for Single Cell Multiome ATAC + Gene Expression Sequencing (User Guide, CG000375 Rev B). Each sample was filtered through a 40µm cell strainer prior to FACS sorting. Sorted and permeabilized nuclei were pelleted at 500xg for 5 min at 4°C, counted and used for Chromium Single Cell Multiome ATAC + Gene Expression library preparation.

Cell sorting

The stained cell nuclei suspension samples were then analyzed and sorted utilizing a BD Bioscience Influx flow cytometer using an 86 μm nozzle. Flow cytometry analyses and sorting were carried out by the following gating strategy: nuclei:singlets:7-AAD positive events. The nuclei sub-population was characterized in the Side Scatter-Forward Scatter plot by back-gating from the 7-AAD (ex. 488 nm, em. 692 nm), singlets were gated in the Side Scatter – Pulse width plot and finally the nuclei were gated in the Side Scatter – 7-AAD plot. The nuclei were collected in a BSA coated Eppendorf tube.

Single nuclei samples

Isolated and sorted nuclei were used to generate single nuclei gene expression and ATAC libraries according to the manufacturer's protocol using Chromium Single Cell Multiome ATAC + Gene Expression kit (User Guide, CG000338 Rev E). Finished Gene Expression libraries were sequenced by using an Illumina NextSeq2000 platform with lengths of read 1 and read 2, 28 bp and 120 bp long respectively. Finished ATAC libraries were sequenced by using an Illumina NextSeq2000 platform. Length of both read 1 and read 2 was 50 bp long.

Pre-processing and Clustering of of Spatial Transcriptomics (ST) and multiomics Data

ST Data generation

Sequenced Visium libraries were processed using Space Ranger software (version 1.0.0, 10X Genomics). Reads were aligned to the Space Ranger built-in mouse reference genome (mm10-3.0.0) and count matrices were generated using these along with the Hematoxylin and Eosin (H&E) images.

ST data analysis

The count matrices were enriched for protein-coding and lincRNA genes and then filtered for MALAT1, ribosomal and mitochondrial genes. Next, all spots containing less than 200 were removed. Technical variability within data was reduced with RunSCT (default settings) and RunHarmony (default settings) functions. Downstream analysis was performed jointly using the Seurat package (v4.0.1) and STUtility (v0.1.0). Principal Component Analysis (PCA) was used for selection of significant components. Uniform Manifold Approximation and Projection (UMAP) was used to visualize ST clusters (resolution=0.35, dims=1:35).

Multiomics data generation

Sequenced single nuclei RNA/ATAC-seq libraries were processed using CellRanger ARC (v2) software from 10X Genomics with default settings. Reads were mapped to the mouse genome (mm10 reference 2020-A from 10X Genomics). Data was then analyzed using the Seurat (v4.1.0) and Signac (v1.6.0) packages.

Multiomics data analysis

In total, extracted single nuclei from 5 brain hemispheres were processed, resulting in 21,178 nuclei used in the analysis. MALAT1, ribosomal and mitochondrial genes were removed and count matrix was further filtered on number of reads, genes and peaks, as well as fraction ATAC-seq reads in peaks, and enrichment of ATAC-seq reads at transcription start sites. Doublet finder was used for doublet removal (v2.0.3) with a doublet score cut-off of 0.6. RNA-seq data was normalized using SCTransform with V2 regularization, while also regressing out cell cycle effects. ATAC-seq data was normalized using TF-IDF normalization. Harmony

(group.by.vars=‘‘bio_origin’’) was then used to integrate data from different samples, after which cells were clustered based on both RNA-seq and ATAC-seq data, using Weighted Nearest Neighbor (WNN) Analysis. Uniform Manifold Approximation and Projection (UMAP) was used to visualize ST clusters (resolution=0.3; dims=2:20), for identification of differentially expressed genes between cluster function FindAllMarkers from Seurat package. To detect differentially expressed genes between flight and ground conditions, while taking biological variation between the different samples into account, MAST with a mixed model, with sample as a random effect was used.

Differential Expression Analysis

For identification of differentially expressed genes between clusters FindAllMarkers() from Seurat was used. Differential gene expression analysis between conditions (flight vs. ground control) was performed using MAST (v1.20.0) with a mixed model, using sample as a random effect.

Gene annotation

Marker genes from the clustering analysis and the DEGs from the differential expression, for both ST and multiomics data, were annotated using previously known marker genes and their functions found from http://mousebrain.org [66] and the web-based tool EnrichR (https://maayanlab.cloud/Enrichr/) [67–69].

Pathway analysis

For pathway analysis and visualization of the results, pathway consensus analysis platform was used (https://bioinformatics.cse.unr.edu/software/cpa/).

Ligand-receptor analysis

Ligand-receptor interactions analysis was performed with the package CellPhoneDB (v3) [70]. Multiomics clusters were analyzed using the DE genes for spaceflight obtained from using MAST (see 'Differential Expression Analysis' in **Methods**).

Spatial pattern analysis

We inferred a gene regulatory network (GRN) from the brain multiomics dataset using CellOracle [46]. A tissue-specific GRN was generated by grouping all brain cell types into the same label before running the method. Transcription Factor (TF) activities were inferred for the brain spatial transcriptomics data using decoupler-py [44] with the method mlm and the obtained GRN as prior knowledge. Additionally, pathway activities were inferred for the brain spatial transcriptomics data using decoupler-py with the method mlm and the PROGENy model of pathway footprints as prior knowledge [45].

To analyze spatial relationships between cell types and pathway activities, we built cell type specific models with MISTy [43], which predict abundances (as determined by Stereoscope) from pathway activities in situ and from the local neighborhood (up to two spots away). In this case, The MISTy models are built only on Visium spots with at least 5% of the specific cell type. We then extracted cell type-pathway interactions that occur in only one of the conditions. In the regions of interest where these differential interactions occur, we investigate changes in correlation (Pearson) between pathway activities and TF activities inferred from the CellOracle GRNs. We

use Student's t-tests with Benjamini-Hochberg multiple testing correction for both determining the differential interactions and the changes in correlation.

Metabolic Pathway Analysis

The flight-vs-ground expression level fold changes of each cluster were computed for genes that are expressed in more than 1% of the cells in either flight or ground condition of the cluster, using the FindMarkers function in the Seurat package (v4.1.1) [71]. Genes listed in the RECON3D metabolic model [72] were extracted with their assigned metabolic pathway membership. The human gene IDs were translated to mouse gene IDs using the manual inspection and the HUGO Gene Nomenclature Committee (HGNC) Comparison of Orthology Predictions (HCOP) service [73]. All genes from the flight-vs-ground expression analysis were then ranked by fold-change differences (positive to negative) regardless of the p-value from FindMarkers function, and tested for pathway enrichment vs the genes in RECON3D pathways using the fgsea function in the fgsea_1.22.0 package [74] in R (v4.2.1; 2022-06-23) [75]. Resulting p-value enrichment of RECON3D-sourced pathways were adjusted (adjusted p-value) by program for the number of pathway tests performed.

Ethical approval

The study followed recommendations in the Guide for the Care and Use of Laboratory Animals and the protocol was approved by the NASA Flight Institutional Animal Care and Use Committee (IACUC).

Data availability

Raw fastq files for ST, snRNA-seq and snATAC-seq data, processed data (aggregated gene count matrices and fragment files) from multiomics dataset, corresponding brightfield images from the ST dataset, and associated metadata are available under the OSD-352 study hosted on the NASA GeneLab server which can be accessed publicly via the DOI link: https://doi.org/10.26030/jm59-zy54 upon publication. At present, all submitted data under the OSD-352 study can be viewed via a private preview link: https://osdr.nasa.gov/bio/repo/data/studies/OSD-352/preview/mxilR7bds8CRIL7REPejBBJppeini1S-. Processed count matrices for the ST samples, final seurat objects (both ST and multiomics), metadata and the deconvolution results are accessible from Mendeley dataset via https://data.mendeley.com/datasets/fjxrcbh672/draft?a=69394d54-235c-436e-be60-520cd2899517 which will also be publicly accessible upon publication.

Code availability

All the necessary scripts required for the generation, processing, and analysis of the data discussed in this manuscript can be accessed via our publicly available repository on Github: https://github.com/giacomellolab/NASA_RR3_Brain. Interactive visualization of our dataset can be done via our shiny app: https://giacomellolabst.shinyapps.io/rr3-brain-shiny/.

References

1. Afshinnekoo, E. *et al.* Fundamental Biological Features of Spaceflight: Advancing the Field to Enable Deep-Space Exploration. *Cell* **183**, 1162–1184 (2020).

2. Li, Z. *et al.* Exposure to galactic cosmic radiation compromises DNA repair and increases the potential for oncogenic chromosomal rearrangement in bronchial epithelial cells. *Sci. Rep.* **8**, 11038 (2018).
3. Juhl, O. J., 4th *et al.* Update on the effects of microgravity on the musculoskeletal system. *NPJ Microgravity* **7**, 28 (2021).
4. Willey, J. S., Lloyd, S. A. J., Nelson, G. A. & Bateman, T. A. Space Radiation and Bone Loss. *Gravit. Space Biol. Bull.* **25**, 14–21 (2011).
5. Guo, J.-H. *et al.* Keeping the right time in space: importance of circadian clock and sleep for physiology and performance of astronauts. *Mil Med Res* **1**, 23 (2014).
6. Turroni, S. *et al.* Gut Microbiome and Space Travelers' Health: State of the Art and Possible Pro/Prebiotic Strategies for Long-Term Space Missions. *Front. Physiol.* **11**, 553929 (2020).
7. Strollo, F., Gentile, S., Strollo, G., Mambro, A. & Vernikos, J. Recent Progress in Space Physiology and Aging. *Front. Physiol.* **9**, 1551 (2018).
8. Overbey, E. G. *et al.* Spaceflight influences gene expression, photoreceptor integrity, and oxidative stress-related damage in the murine retina. *Sci. Rep.* **9**, 13304 (2019).
9. Mao, X. W. *et al.* Spaceflight induces oxidative damage to blood-brain barrier integrity in a mouse model. *FASEB J.* **34**, 15516–15530 (2020).
10. Overbey, E. G. *et al.* Mice Exposed to Combined Chronic Low-Dose Irradiation and Modeled Microgravity Develop Long-Term Neurological Sequelae. *Int. J. Mol. Sci.* **20**, (2019).
11. Holley, J. M. *et al.* Characterization of gene expression profiles in the mouse brain after 35 days of spaceflight mission. *NPJ Microgravity* **8**, 35 (2022).

12. Cekanaviciute, E., Rosi, S. & Costes, S. V. Central Nervous System Responses to Simulated Galactic Cosmic Rays. *Int. J. Mol. Sci.* **19**, (2018).
13. Vernice, N. A., Meydan, C., Afshinnekoo, E. & Mason, C. E. Long-term spaceflight and the cardiovascular system. *Precis Clin Med* **3**, 284–291 (2020).
14. Lee, J. K. *et al.* Spaceflight-Associated Brain White Matter Microstructural Changes and Intracranial Fluid Redistribution. *JAMA Neurol.* **76**, 412–419 (2019).
15. Patel, Z. S. *et al.* Red risks for a journey to the red planet: The highest priority human health risks for a mission to Mars. *NPJ Microgravity* **6**, 33 (2020).
16. Wang, Y. & Navin, N. E. Advances and applications of single-cell sequencing technologies. *Mol. Cell* **58**, 598–609 (2015).
17. Ståhl, P. L. *et al.* Visualization and analysis of gene expression in tissue sections by spatial transcriptomics. *Science* **353**, 78–82 (2016).
18. Overbey, E. G. *et al.* Challenges and considerations for single-cell and spatially resolved transcriptomics sample collection during spaceflight. *Cell Rep Methods* **2**, 100325 (2022).
19. Nguyen, H. *et al.* CPA: a web-based platform for consensus pathway analysis and interactive visualization. *Nucleic Acids Res.* **49**, W114–W124 (2021).
20. Calabrese, G., Molzahn, C. & Mayor, T. Protein interaction networks in neurodegenerative diseases: From physiological function to aggregation. *J. Biol. Chem.* **298**, 102062 (2022).
21. Sušjan-Leite, P., Ramuta, T. Ž., Boršić, E., Orehek, S. & Hafner-Bratkovič, I. Supramolecular organizing centers at the interface of inflammation and neurodegeneration. *Front. Immunol.* **13**, 940969 (2022).
22. Andersson, A. *et al.* Single-cell and spatial transcriptomics enables probabilistic inference of cell type topography. *Commun Biol* **3**, 565 (2020).

668 23. Marchionini, D. M. *et al.* Role of heparin binding growth factors in nigrostriatal dopamine
669 system development and Parkinson's disease. *Brain Res.* **1147**, 77–88 (2007).
670 24. Romano, R. & Bucci, C. Role of EGFR in the Nervous System. *Cells* **9**, (2020).
671 25. Licht, T. & Keshet, E. Delineating multiple functions of VEGF-A in the adult brain. *Cell.*
672 *Mol. Life Sci.* **70**, 1727–1737 (2013).
673 26. Meissirel, C. *et al.* VEGF modulates NMDA receptors activity in cerebellar granule cells
674 through Src-family kinases before synapse formation. *Proc. Natl. Acad. Sci. U. S. A.* **108**,
675 13782–13787 (2011).
676 27. Argaw, A. T. *et al.* Astrocyte-derived VEGF-A drives blood-brain barrier disruption in CNS
677 inflammatory disease. *J. Clin. Invest.* **122**, 2454–2468 (2012).
678 28. Welle, A. *et al.* Epigenetic control of region-specific transcriptional programs in mouse
679 cerebellar and cortical astrocytes. *Glia* **69**, 2160–2177 (2021).
680 29. Aruga, J., Inoue, T., Hoshino, J. & Mikoshiba, K. Zic2 controls cerebellar development in
681 cooperation with Zic1. *J. Neurosci.* **22**, 218–225 (2002).
682 30. Ikushima, H. *et al.* Glioma-initiating cells retain their tumorigenicity through integration of
683 the Sox axis and Oct4 protein. *J. Biol. Chem.* **286**, 41434–41441 (2011).
684 31. Di Stefano, B., Prigione, A. & Broccoli, V. Efficient genetic reprogramming of unmodified
685 somatic neural progenitors uncovers the essential requirement of Oct4 and Klf4. *Stem Cells*
686 *Dev.* **18**, 707–716 (2009).
687 32. Graham, V., Khudyakov, J., Ellis, P. & Pevny, L. SOX2 functions to maintain neural
688 progenitor identity. *Neuron* **39**, 749–765 (2003).
689 33. Simeone, A. Genetic control of dopaminergic neuron differentiation. *Trends Neurosci.* **28**,
690 62–5; discussion 65–6 (2005).

34. Wu, J.-S., Tsai, H.-D., Cheung, W.-M., Hsu, C. Y. & Lin, T.-N. PPAR-γ Ameliorates Neuronal Apoptosis and Ischemic Brain Injury via Suppressing NF-κB-Driven p22phox Transcription. *Mol. Neurobiol.* **53**, 3626–3645 (2016).
35. Zhao, X.-R., Gonzales, N. & Aronowski, J. Pleiotropic role of PPARγ in intracerebral hemorrhage: an intricate system involving Nrf2, RXR, and NF-κB. *CNS Neurosci. Ther.* **21**, 357–366 (2015).
36. Hermann-Kleiter, N. *et al.* The nuclear orphan receptor NR2F6 suppresses lymphocyte activation and T helper 17-dependent autoimmunity. *Immunity* **29**, 205–216 (2008).
37. Chen, W. Y. *et al.* Tumor suppressor HIC1 directly regulates SIRT1 to modulate p53-dependent DNA-damage responses. *Cell* **123**, 437–448 (2005).
38. Sahar, S. & Sassone-Corsi, P. Metabolism and cancer: the circadian clock connection. *Nat. Rev. Cancer* **9**, 886–896 (2009).
39. Kawai, M. *et al.* Nocturnin: a circadian target of Pparg-induced adipogenesis. *Ann. N. Y. Acad. Sci.* **1192**, 131–138 (2010).
40. Bahrami-Nejad, Z. *et al.* A Transcriptional Circuit Filters Oscillating Circadian Hormonal Inputs to Regulate Fat Cell Differentiation. *Cell Metab.* **27**, 854–868.e8 (2018).
41. Liu, Y., Niu, L., Liu, X., Cheng, C. & Le, W. Recent Progress in Non-motor Features of Parkinson's Disease with a Focus on Circadian Rhythm Dysregulation. *Neurosci. Bull.* **37**, 1010–1024 (2021).
42. Warnecke, M., Oster, H., Revelli, J.-P., Alvarez-Bolado, G. & Eichele, G. Abnormal development of the locus coeruleus in Ear2(Nr2f6)-deficient mice impairs the functionality of the forebrain clock and affects nociception. *Genes Dev.* **19**, 614–625 (2005).

43. Tanevski, J., Flores, R. O. R., Gabor, A., Schapiro, D. & Saez-Rodriguez, J. Explainable multiview framework for dissecting spatial relationships from highly multiplexed data. *Genome Biol.* **23**, 97 (2022).
44. Badia-i-Mompel, P. *et al.* decoupleR: ensemble of computational methods to infer biological activities from omics data. *Bioinformatics Advances* **2**, (2022).
45. Schubert, M. *et al.* Perturbation-response genes reveal signaling footprints in cancer gene expression. *Nat. Commun.* **9**, 20 (2018).
46. Kamimoto, K., Hoffmann, C. M. & Morris, S. A. CellOracle: Dissecting cell identity via network inference and in silico gene perturbation. *bioRxiv* 2020.02.17.947416 (2020) doi:10.1101/2020.02.17.947416.
47. Subramanian, A. *et al.* Gene set enrichment analysis: a knowledge-based approach for interpreting genome-wide expression profiles. *Proc. Natl. Acad. Sci. U. S. A.* **102**, 15545–15550 (2005).
48. Mootha, V. K. *et al.* PGC-1alpha-responsive genes involved in oxidative phosphorylation are coordinately downregulated in human diabetes. *Nat. Genet.* **34**, 267–273 (2003).
49. da Silveira, W. A. *et al.* Comprehensive Multi-omics Analysis Reveals Mitochondrial Stress as a Central Biological Hub for Spaceflight Impact. *Cell* **183**, 1185–1201.e20 (2020).
50. Rao, J. S., Rapoport, S. I. & Kim, H.-W. Altered neuroinflammatory, arachidonic acid cascade and synaptic markers in postmortem Alzheimer's disease brain. *Transl. Psychiatry* **1**, e31 (2011).
51. Amtul, Z., Uhrig, M., Wang, L., Rozmahel, R. F. & Beyreuther, K. Detrimental effects of arachidonic acid and its metabolites in cellular and mouse models of Alzheimer's disease: structural insight. *Neurobiol. Aging* **33**, 831.e21–31 (2012).

52. Stella, N., Tencé, M., Glowinski, J. & Prémont, J. Glutamate-evoked release of arachidonic acid from mouse brain astrocytes. *J. Neurosci.* **14**, 568–575 (1994).
53. Trostchansky, A. *et al.* Profile of Arachidonic Acid-Derived Inflammatory Markers and Its Modulation by Nitro-Oleic Acid in an Inherited Model of Amyotrophic Lateral Sclerosis. *Front. Mol. Neurosci.* **11**, 131 (2018).
54. Blaber, E. A. *et al.* Microgravity induces pelvic bone loss through osteoclastic activity, osteocytic osteolysis, and osteoblastic cell cycle inhibition by CDKN1a/p21. *PLoS One* **8**, e61372 (2013).
55. Ma, C. *et al.* Simulated Microgravity Potentiates Hematopoietic Differentiation of Human Pluripotent Stem Cells and Supports Formation of 3D Hematopoietic Cluster. *Front Cell Dev Biol* **9**, 797060 (2021).
56. Parihar, V. K. *et al.* Cosmic radiation exposure and persistent cognitive dysfunction. *Sci. Rep.* **6**, 34774 (2016).
57. Flynn-Evans, E. E., Barger, L. K., Kubey, A. A., Sullivan, J. P. & Czeisler, C. A. Circadian misalignment affects sleep and medication use before and during spaceflight. *NPJ Microgravity* **2**, 15019 (2016).
58. Dijk, D.-J. *et al.* Sleep, performance, circadian rhythms, and light-dark cycles during two space shuttle flights. *American Journal of Physiology-Regulatory, Integrative and Comparative Physiology* **281**, R1647–R1664 (2001).
59. Inokawa, H. *et al.* Chronic circadian misalignment accelerates immune senescence and abbreviates lifespan in mice. *Sci. Rep.* **10**, 2569 (2020).
60. Crucian, B. E. *et al.* Immune System Dysregulation During Spaceflight: Potential Countermeasures for Deep Space Exploration Missions. *Front. Immunol.* **9**, 1437 (2018).

61. Takamatsu, Y. *et al.* Protection against neurodegenerative disease on Earth and in space. *npj Microgravity* **2**, 1–4 (2016).
62. Nelson, C. A. *et al.* Knowledge Network Embedding of Transcriptomic Data from Spaceflown Mice Uncovers Signs and Symptoms Associated with Terrestrial Diseases. *Life* **11**, (2021).
63. Mu, X. *et al.* Small tissue chips with big opportunities for space medicine. *Life Sci. Space Res.* **35**, 150–157 (2022).
64. Yeung, C. K. *et al.* Tissue Chips in Space-Challenges and Opportunities. *Clin. Transl. Sci.* **13**, 8–10 (2020).
65. Verma, S. D. *et al.* Astrocytes regulate vascular endothelial responses to simulated deep space radiation in a human organ-on-a-chip model. *Front. Immunol.* **13**, 864923 (2022).
66. La Manno, G. *et al.* Molecular architecture of the developing mouse brain. *Nature* **596**, 92–96 (2021).
67. Chen, E. Y. *et al.* Enrichr: interactive and collaborative HTML5 gene list enrichment analysis tool. *BMC Bioinformatics* **14**, 128 (2013).
68. Kuleshov, M. V. *et al.* Enrichr: a comprehensive gene set enrichment analysis web server 2016 update. *Nucleic Acids Res.* **44**, W90–7 (2016).
69. Xie, Z. *et al.* Gene Set Knowledge Discovery with Enrichr. *Curr Protoc* **1**, e90 (2021).
70. Garcia-Alonso, L. *et al.* Mapping the temporal and spatial dynamics of the human endometrium in vivo and in vitro. *Nat. Genet.* **53**, 1698–1711 (2021).
71. Hao, Y. *et al.* Integrated analysis of multimodal single-cell data. *Cell* **184**, 3573–3587.e29 (2021).

72. Brunk, E. *et al.* Recon3D enables a three-dimensional view of gene variation in human metabolism. *Nat. Biotechnol.* **36**, 272–281 (2018).
73. Eyre, T. A., Wright, M. W., Lush, M. J. & Bruford, E. A. HCOP: a searchable database of human orthology predictions. *Brief. Bioinform.* **8**, 2–5 (2007).
74. Korotkevich, G. *et al.* Fast gene set enrichment analysis. *bioRxiv* 060012 (2021) doi:10.1101/060012.
75. The R Project for Statistical Computing. https://www.r-project.org/.

Declarations

Acknowledgements

We would like to gratefully acknowledge the assistance of San-huei Lai Polo with hosting data on the NASA GeneLab server. We thank Uppsala Multidisciplinary Center for Advanced Computational Science (UPPMAX) for providing computational infrastructure. This study was supported by NASA GeneLab. S.G. was supported by Formas grant 2017-01066 and VR grant 2020-04864. The authors would also like to thank NASA Ames Research Center for providing the mouse samples to carry out this study.

Author contributions

Conceptualization: SG, JMG, SVC. **Methodology**: SG. **Investigation**: ZA performed ST and single-cell multiomics experiments; VB performed sequencing, EL performed nuclei isolation. **Formal analysis**: EC performed data annotation, ZA and ÅB performed ST data analysis, JOW

performed single-cell multiomics analysis, RF and PBiM performed MISTy analysis, SV and DT performed pathway analysis, CS performed Ligand-Receptor analysis. **Validation**: RF, PBiM and DCW. **Software**: JOW, ÅB. **Resources**: VB, ASB, DCW, JMG, SVC. **Data curation**: JOW, ÅB, ASB, CS, RF and PBiM. **Visualization**: YM, ZA, CS. **Supervision**: SG, OB, JSR, JMG. **Project administration**: SG, SamrawitG, JMG, SVC. **Funding acquisition:** SVC, SG. **Writing – original draft**: YM, EC, ZA, DT, DCW and SG. **Writing – review & editing**: All authors.

Competing interests

ZA and SG are scientific advisors to 10x Genomics Inc, which holds IP rights to the ST technology. S.G. holds 10X Genomics stock options. All other authors declare no competing interests.

Additional Information

Correspondence and requests for materials should be addressed to Stefania Giacomello.

Additional File 1: Portable Document Format (PDF), Supplementary Information:

Supplementary Figures and Supplementary Table legends.

Additional File 2: Office Open XML Workbook (XLSX): Supplementary Table 1.

Additional File 3: Office Open XML Workbook (XLSX): Supplementary Table 2.

Additional File 4: Office Open XML Workbook (XLSX): Supplementary Table 3.

Additional File 5: Office Open XML Workbook (XLSX): Supplementary Table 4.

Additional File 6: Office Open XML Workbook (XLSX): Supplementary Table 5.

Additional File 7: Office Open XML Workbook (XLSX): Supplementary Table 6.

Additional File 8: Office Open XML Workbook (XLSX): Supplementary Table 7.

Additional File 9: Office Open XML Workbook (XLSX): Supplementary Table 8.

Additional File 10: Office Open XML Workbook (XLSX): Supplementary Table 9.

Additional File 11: Office Open XML Workbook (XLSX): Supplementary Table 10.

Supplementary Files

This is a list of supplementary files associated with this preprint. Click to download.

- SupplementaryTable1.xlsx
- SupplementaryTable2.xlsx
- SupplementaryTable3.xlsx
- SupplementaryTable4.xlsx
- SupplementaryTable5.xlsx
- SupplementaryTable6.xlsx
- SupplementaryTable7.xlsx
- SupplementaryTable8.xlsx
- SupplementaryTable9.xlsx
- SupplementaryTable10.xlsx
- SupplementaryInformation.pdf